Electromagnetic Detection and Real-Time DMLC Adaptation to Target Rotation During Radiotherapy

Junqing Wu, M.S.,[1,2] Dan Ruan, Ph.D.,[1] Byungchul Cho, Ph.D.,[1,3] Amit Sawant, Ph.D.,[1] Jay Petersen, M.S.,[4] Laurence J. Newell, M.S.,[4] Herbert Cattell, M.S.,[5] and Paul J. Keall, Ph.D.[1,6]

1. Department of Radiation Oncology, Stanford University, Stanford, CA
2. School of Health Sciences, Purdue University, West Lafayette, IN
3. Asan Medical Center, Seoul, Korea
4. Calypso Medical Technologies, Seattle, WA
5. Varian Medical Systems, Palo Alto, CA
6. Radiation Physics Laboratory, Sydney Medical School, University of Sydney, Sydney, Australia

Corresponding Author: Paul J. Keall, Ph.D., Sydney Medical School, University of Sydney, NSW 2006, Australia. Tel: þ61 2 9351 3590; Fax: þ61 2 9351 4018; E-mail: radphyslab@sydney.edu.au

Conflicts of interest: There are authors from two companies, Calypso and Varian, who provided scientific and engineering input into this work. Research support was received from Calypso, Varian, and NIH R01 93626 is gratefully acknowledged.

Acknowledgments: The authors thank both Libby Roberts (Stanford) and Julie Baz (Sydney) for reviewing the manuscript and improving the clarity.

Keywords

Tumor rotation, Tumor tracking, Real-time Intrafraction motion

Summary

Current-day radiotherapy systems do not account for tumor rotation, and dosimetric errors may result. This study reports a system that integrates a prototype electromagnetic tracking system to detect tumor translation and rotation with a dynamic multileaf collimator system that in real-time adapts the radiation beam to the translation and rotating tumor. Results show a rotation accuracy correction error of less than 1 degree. Dosimetric studies showed a three-fold improvement in target dose accuracy compared to current-day clinically available technology.

Introduction

Tumor motion can significantly influence the accuracy of radiation therapy. Therefore, margins are included in the planning target volume to account for the range of target motion. This expansion ensures tumor coverage, but also leads to higher dose to normal tissue. To reduce these margins, dynamic multileaf collimator (DMLC) tracking has been investigated because it can achieve high-dose conformality with minimal sacrifice of treatment efficiency.

In the past few years, researchers have empirically investigated DMLC tracking on a variety of commercial platforms including AccuKnife (1), Siemens (2), Tomotherapy (3, 4,) and Varian (5, 6, 7, 8). This work to date has focused on adapting to translational motion of the targets. Rotational target motion has not previously been studied. However, lung tumors and prostate tumors have been observed to rotate as much as 45° and 25°, respectively (9, 10). Significant rotations have also been reported for liver tumors and a gastrointestinal stromal tumor during respiration (11, 12). Table 1 summarizes tumor rotational movement studies for a variety of tumor sites.

As with translational motion, rotational motion can severely compromise target dose coverage and normal tissue sparing if it is not accounted for. Rotation may cause part of the target volume to move out of the treatment field and result in underdose (13, 14). Recently, Li et al. (15) found that the dosimetric discrepancies caused by prostate rotation were more significant than those caused by translational intrafractional motion. They concluded that treatment margins may be reduced significantly if the prostate rotation can be controlled to within 1° in all directions.

Strategies of rotational motion correction for intensity-modulated radiation therapy (IMRT) treatment have been studied (14, 16, 17, 18) and gantry, collimator, and/or couch angle adjustment has been proposed. However, existing studies are limited to interfraction rotational motion and require manual intervention for each beam during radiation therapy delivery and are not real-time. The aim of the current study was to investigate and evaluate the geometric and dosimetric performance of an electromagnetically guided real-time DMLC tracking system to detect and adapt to intrafractional tumor rotation.

Methods and Materials

Electromagnetically guided real-time DMLC tracking system

A research four-dimensional localization system (Calypso Medical Technologies Inc., Seattle, WA) was integrated with a real-time DMLC tracking system employed on a Varian IX linear

accelerator (Varian Medical System, Palo Alto, CA) with a 120-leaf MLC, which has previously been used for studying DMLC tracking in the presence of translational motion (19, 20, 21). In this work, the four-dimensional localization system electromagnetically measured the positions of the transponders and provided the target translation and rotation information. The data stream was input to the DMLC tracking software, where the beam aperture generated by the treatment planning system (and indexed by monitor units for IMRT) was translated and rotated based on the data stream values to generate an ideal aperture. This ideal aperture was typically undeliverable, because of physical constraints such as finite MLC leaf widths, and more importantly the paired leaf structure. An optimization framework was used to find, among all deliverable MLC configurations, the one that is closest to the ideal aperture, where closeness is defined rigorously as the cumulative cost in terms of underdose (to target) and overdose (to healthy tissue) (22). The translation and rotation adapted MLC configuration was sent to the DMLC controller. The time delay of the system was measured to be 193 ms (19). No prediction algorithm was used to account for the time delay as the algorithms in the prototype system currently only predict translational motion.

Geometric study

The experimental setup is shown in Fig. 1 and Fig. 2. To test the geometric accuracy, three 3-mm-diameter tungsten balls (hereafter referred to as "markers") were embedded in a puck, along with implanted electromagnetic transponders. Ciné electronic portal imaging device (EPID) images at 10.5 Hz were acquired for a D-shape aperture beam, from which the beam aperture and the positions of radio-opaque markers were simultaneously observed. The EPID is an appropriate measuring tool for this study as it can independently observe the target and beam rotation. A Matlab (Mathworks, Natick, MA) program was written to process EPID images and analyze the match between target rotation and MLC beam aperture rotation. This application automatically extracted the marker positions from EPID images and calculated the target rotation angle. The observed marker configuration provided the “ground-truth” for an instantaneous target rotation angle, whereas the extracted orientation of the beam aperture represented the tracking results. Both the target positions and beam aperture were detected using threshold-based segmentation methods. The beam aperture rotation angle was estimated from the slope of straight sideline on the D-shape beam (Fig. 3). The discrepancy between these two angular quantities, the beam-target rotational alignment difference, was used as the performance metric for geometric accuracy.

Both fixed rotation and active rotation were studied. Here, fixed rotated target signifies the target is rotated prior to treatment and does not move during treatment, and actively rotating target signifies that the target is rotating during treatment. The rotation angle values were chosen to span the largest (to date) observed rotation, 46° (Table 1). For fixed rotation, the phantom was rotated to a group of preset angles (5–55° in 5° increments) by rotating the couch. At least 10

EPID images were acquired at each couch angle. EPID images of DMLC aperture tracking for the target rotated to 0°, 10°, 20°, 30°, 40°, and 50° are shown in Fig. 4. For dynamic rotation, the couch was rotated continuously from 0° to 60° and from 60° to 0° via control at the treatment console at a speed of approximately 4°/sec. Approximately 40 EPID images were acquired during the dynamic rotation. The gantry angle and collimator angles were kept at 180° (Varian Scale) so that the beam central axis was perpendicular to the rotational plane.

Dosimetric study

The experimental setup for the dosimetric study was the same as the geometric study. A PTW two-dimensional ion chamber array (PTW, Freiburg, Germany) with 2 cm of solid water buildup was placed between the couch and puck with embedded transponders for dosimetric measurement. A magnetic shielding "Faraday cage" (two layers of aluminum foil) was placed around the PTW detectors and cable to reduce the current induced by the electromagnetic array in the ion chamber array. This shielding reduced the leakage dose from 0.3 Gy to 0.003 Gy over 1 min. As in the geometric experiment, the couch was rotated to simulate fixed and active rotational movement of the tumor.

In the dosimetric study, we used a conformal ellipse beam (minor and major axes 5 cm and 7 cm, respectively) and two lung dynamic (sliding window) IMRT beams, because lung tumors have been observed to undergo large rotational motion. For each beam, we tested the following five delivery modes: 1) nonrotated target (reference), during which the target was kept still in the planned position without any rotation—the dosimetric results represent the ideal situation; 2) fixed rotated target with tracking, during which the target was rotated to fixed angles (15°, 30°, 45°, 60°) with active real-time DMLC tracking; 3) fixed rotated target with tracking, during which the target was rotated to fixed angles with no motion adaptation during delivery; 4) active rotating target with tracking; and 5) active rotating target without tracking, during which the target was continuously rotated back and forth at a speed of ∼4°/sec between 0° and 60°. The discrepancy between 1) and 3) and 1) and 5) reflects the dosimetric impact of uncompensated target rotation. Two hundred monitor units were delivered for all beams. Dosimetric performance of the latter four modes was measured and compared with the reference distribution using a 3-mm/3% γ-test with a 5% low-dose threshold, below which differences were ignored. The comparison method is shown in Fig. 5.

Results

The geometric results for fixed rotation and active rotation are shown in Table 2 and Table 3, respectively. Overall, the geometric experimental results indicated that the beam-target rotational alignment difference was 0.3°± 0.6° for fixed rotation and 0.3° ± 1.3° for active rotation. Both results demonstrated sub-2° accuracy for the tracking system with most of the results within ±1°. Because of system latency and the EPID integration time, the beam-target alignment difference

for active rotation was larger than the fixed rotation beam-target alignment difference, as expected, and exhibited directional dependence. Given the 4°/sec rotation and 193-ms system latency, a directionally dependent 0.8° systematic error is estimated for active rotation. This error could be reduced with lower system latency and/or developing a prediction algorithm to estimate rotation.

The dose distribution from fixed rotated target tracking and actively rotating target tracking were similar to that of the reference obtained with a nonrotated target. Example isodose curves of comparing rotation tracking and no rotation tracking to IMRT fields are shown in Fig. 6. The plans delivered without rotation tracking tended to have misshaped and shifted dose distributions compared with the rotation tracking IMRT distributions because of a combination of geometric error and the interplay effect (23). Both the geometric error and interplay effect depend on the starting rotation angle.

The 3-mm/3% γ-test results are shown in Fig. 7. The rotation tracking results demonstrated a significantly better match for all cases. The average failure rate for the γ-test for a fixed rotated target was 11% with tracking and 36% without tracking; the average failure rate for an actively rotating target was 9% with tracking and 35% without tracking.

There was some treatment efficiency loss with DMLC tracking because of beam holds. Beam holds occur when any one of the MLC leaves cannot reach the desired position to within the preset tolerance (0.5 cm for these cases). Table 4 summarizes the treatment efficiency with the change of rotation angle. A larger rotation angle required more MLC position adjustment for the treatment and caused a beam hold because of limited maximum leaf velocities (~3.60 cm/sec) (24, 25), resulting in a longer treatment time for the same monitor unit delivery. Therefore, treatment efficiency decreased as the rotation angle increased. The lowest treatment efficiency with DMLC tracking was 66% when the target was rotated 60°, which is still reasonable for clinical implementation.

Discussion

Electromagnetically guided DMLC adaptation to rotational target motion has been investigated. The geometric accuracy and dose distributions to fixed and actively rotating targets with DMLC tracking were significantly superior to those without tracking. In most cases, the rotational error was within 1°, which—according to an independent prostate study by Li et al.(15)—would allow treatment margins to be reduced significantly. It should also be noted that the geometric and dosimetric results mentioned here represent an upper bound of error. Reductions in measurement error, system latency, and faster and/or thinner MLC leaves, DMLC tracking algorithm improvements, and including rotational prediction would further reduce the geometric and dose differences observed from the ideal nonrotated case.

As expected, when the rotation angle increased from 15° to 60°, the failure rate for the without tracking measurement increased dramatically from 15% to 52%. Larger rotation movement led to larger discrepancy. In contrast, the failure rate for target tracking measurement increased slightly from an average of 8–14% and was more immune to the adverse impact of rotational motion.

The study was limited to rotational movements in the sagittal plane, perpendicular to the beam direction or "in-plane" rotation. A further limitation was that the dynamic rotation used a constant angular velocity of 4°/sec. Future rotation detection and adaptation study is planned for more complex and realistic patient rotation data and more complex delivery, including intensity-modulated ARC therapy delivery. Dedicated phantoms will need to be developed for this purpose.

Currently, the prototype implemented rotation detection and adaptation by using the electromagnetic input data. Electromagnetic-guided tracking is very attractive because it does not give extra radiation dose to patients. However, in principle, other guidance methods that can give rotational motion, including those used for the studies in Table 1, such as kV imaging, MV imaging, ultrasound, and MRI could be integrated with DMLC adaptation, even offering the potential to adapt to target deformation in real time.

An obvious alternate approach to using the DMLC to account for real-time target rotation is to use the existing linear accelerator collimator. Some manufacturers are offering the ability to vary the collimator angle during treatment delivery (though not in a real-time feedback sense). Limitations of using the collimator to account for rotation are the inability to simultaneously account for translation, the collimator rotation velocity limitation (typically 6 or 12°/sec maximum) and the inability to account for out-of-plane rotation (though not included in the current study, out-of-plane rotation can in principle be corrected for via DMLC adaptation). Combining DMLC adaptation with collimator rotation would be an interesting avenue for future research.

One undesirable aspect of DMLC tracking is the increased dose outside the desired field aperture due to the "adjacent closed leaf pairs" (6). These adjacent closed leaf pairs can be seen above and below the open aperture in Fig. 3, Fig. 4. These leaves are not participating in defining the current treatment field, but will define the treatment field if there is a target motion perpendicular to the leaf aperture. The number of adjacent closed leaf pairs is estimated from the extent of

target motion in the perpendicular direction. Two adjacent closed leaf pairs were used for these measurements (the number is a variable within the DMLC tracking software). The impact of these leaves could be reduced with double focused leaves (lower leakage) and faster leaf velocities (fewer adjacent closed leaf pairs needed).

Conclusion

For the first time, real-time target rotation has been accurately detected and adapted to during radiation therapy treatment via DMLC adaptation. The beam-target rotational alignment difference was sub-2°. Dose distributions to rotated and rotating targets with DMLC tracking were significantly superior to those without tracking.

References

1. Liu Y, Shi C, Lin B, et al. Delivery of four-dimensional radiotherapy with TrackBeam for moving target using an AccuKnife dual-layer MLC: Dynamic phantoms study. J Appl Clin Med Phys 2009;10:2926.

2. Tacke M, Nill S, Oelfke U. Real-time tracking of tumor motions and deformations along the leaf travel direction with the aid of a synchronized dynamic MLC leaf sequencer. Phys Med Biol 2007;52: N505eN512.

3. Lu W. Real-time motion-adaptive delivery (MAD) using binary MLC: I. Static beam (topotherapy) delivery. Phys Med Biol 2008;53: 6491e6511.

4. Lu W. Real-time motion-adaptive delivery (MAD) using binary MLC: II. Rotational beam (tomotherapy) delivery. Phys Med Biol 2008;53: 6513e6531.

5. Keall PJ, Cattell H, Pokhrel D, et al. Geometric accuracy of a realtime target tracking system with dynamic multileaf collimator tracking system. Int J Radiat Oncol Biol Phys 2006;65:1579e1584.

6. Sawant A, Venkat R, Srivastava V, et al. Management of threedimensional intrafraction motion through real-time DMLC tracking. Med Phys 2008;35:2050e2061.

7. Poulsen PR, Cho B, Sawant A, et al. Implementation of a new method for dynamic multileaf collimator tracking of prostate motion in arc radiotherapy using a single kV imager. Int J Radiat Oncol Biol Phys 2010;76:914e923.

8. Poulsen PR, Cho B, Ruan D, et al. Dynamic multileaf collimator tracking of respiratory target motion based on a single kilovoltage imager during arc radiotherapy. Int J Radiat Oncol Biol Phys 2010;77: 600e607.

9. Plathow C, Schoebinger M, Fink C, et al. Quantification of lung tumor volume and rotation at 3D dynamic parallel MR imaging with view sharing: Preliminary results. Radiology 2006;240:537e545.

10. Noel CE, Santanam L, Olsen JR, et al. An automated method for adaptive radiation therapy for prostate cancer patients using continuous fiducial-based tracking. Phys Med Biol 2010;55:65e82.

11. Kim G, Shim S, Chung W, et al. The evaluation of tumor motion and treatment accuracy in liver tumor using Synchrony Motion Tracking System. J Korean Soc Ther Radiol Oncol 2008;26:263e270.

12. Ito K, Takahashi Y, Igarashi K, et al. Gastrointestinal stromal tumor with a marked rotation. J Med Ultrasonics 2008;35:75e77.

13. Litzenberg D, Hadley S, Vineber K, et al. Patient-specific rotational tolerances and margins based on prostate shape. Med Phys 2010;37: 3190.

14. van Herten YR, van de Kamer JB, van Wieringen N, et al. Dosimetric evaluation of prostate rotations and their correction by couch rotations. Radiother Oncol 2008;88:156e162.

15. Li JS, Jin L, Pollack A, et al. Gains from real-time tracking of prostate motion during external beam radiation therapy. Int J Radiat Oncol Biol Phys 2009;75:1613e1620.

16. Hoogeman MS, van Herk M, de Bois J, et al. Strategies to reduce the systematic error due to tumor and rectum motion in radiotherapy of prostate cancer. Radiother Oncol 2005;74:177e185.

17. Rijkhorst EJ, van Herk M, Lebesque JV, et al. Strategy for online correction of rotational organ motion for intensity-modulated radiotherapy of prostate cancer. Int J Radiat Oncol Biol Phys 2007;69: 1608e1617.

18. Krauss A, Nill S, Tacke M, et al. Electromagnetic real-time tumor position monitoring and dynamic multileaf collimator tracking using a Siemens 160 MLC: Geometric and dosimetric accuracy of an integrated system. Int J Radiat Oncol Biol Phys 2011;79: 579e587.

19. Sawant A, Smith RL, Venkat RB, et al. Toward submillimeter accuracy in the management of intrafraction motion: The integration of real-time internal position monitoring and multileaf collimator target tracking. Int J Radiat Oncol Biol Phys 2009;74:575e582.

20. Smith RL, Sawant A, Santanam L, et al. Integration of real-time internal electromagnetic position monitoring coupled with dynamic multileaf collimator tracking: An intensity-modulated radiation therapy feasibility study. Int J Radiat Oncol Biol Phys 2009;74: 868e875.

21. Keall PJ, Sawant A, Cho B, et al. Electromagnetic-guided dynamic multileaf collimator tracking enables motion management for intensity-modulated arc therapy. Int J Radiat Oncol Biol Phys 2011; 79:312e320.

22. Ruan D, Poulsen P, Cho B, et al. A novel optimization based leaf sequencing algorithm with explicit underdose and overdose penalties in 4D radiotherapy. Int J Radiat Oncol Biol Phys 2009;75:S627.

23. Yu CX, Jaffray DA, Wong JW. The effects of intra-fraction organ motion on the delivery of dynamic intensity modulation. Phys Med Biol 1998;43:91e104.

24. Poulsen PR, Cho B, Sawant A, et al. Detailed analysis of latencies in image-based dynamic MLC tracking. Med Phys 2010;37:4998e5005.

25. Wijesooriya K, Bartee C, Siebers JV, et al. Determination of maximum leaf velocity and acceleration of a dynamic multileaf collimator: Implications for 4D radiotherapy. Med Phys 2005;32:932e941.

26. Gutfeld O, Kretzler AE, Kashani R, et al. Influence of rotations on dose distributions in spinal stereotactic body radiotherapy (SBRT). Int J Radiat Oncol Biol Phys 2009;73:1596e1601.

27. de Boer HC, van Os MJ, Jansen PP, et al. Application of the No Action Level (NAL) protocol to correct for prostate motion based on electronic portal imaging of implanted markers. Int J Radiat Oncol Biol Phys 2005;61:969e983.

28. Aubry JF, Beaulieu L, Girouard LM, et al. Measurements of intrafraction motion and interfraction and intrafraction rotation of prostate by three-dimensional analysis of daily portal imaging with radiopaque markers. Int J Radiat Oncol Biol Phys 2004;60:30e39.

29. Burch D, Willoughby T, Meeks S, et al. Real time prostate translation, rotation, deformation evaluated with calypso beacon transponders. Int J Radiat Oncol Biol Phys 2005;63:S195.

30. Dehnad H, Nederveen AJ, van der Heide UA, et al. Clinical feasibility study for the use of implanted gold seeds in the prostate as reliable positioning markers during megavoltage irradiation. Radiother Oncol 2003;67:295e302.

31. van der Heide UA, Kotte AN, Dehnad H, et al. Analysis of fiducial marker-based position verification in the external beam radiotherapy of patients with prostate cancer. Radiother Oncol 2007;82:38e45.

32. Balter JM, Sandler HM, Lam K, et al. Measurement of prostate movement over the course of routine radiotherapy using implanted markers. Int J Radiat Oncol Biol Phys 1995;31:113e118.

33. Beck J, Skykes J, Amer A, et al. Precision of prostate translation and rotation measurement from 3D marker localization using orthogonal EPID Images. Radiother Oncol 2004;73:S225.

34. Stroom JC, Koper PC, Korevaar GA, et al. Internal organ motion in prostate cancer patients treated in prone and supine treatment position. Radiother Oncol 1999;51:237e248.

35. Steenbakkers RJ, Duppen JC, Betgen A, et al. Impact of knee support and shape of tabletop on rectum and prostate position. Int J Radiat Oncol Biol Phys 2004;60:1364e1372.

Table 1 Summary of tumor rotation measurement studies

Study first author (Reference)	Tumor site	Measurement method	Number of patients	Comments	Rotation (°)		
					LR	CC	AP
Plathow (9)	Lung	MRI	5 patients	Maximum 46°	25.4 ± 13.4	18.9 ± 11.8	23.1 ± 8.5
Kim (11)	Liver	X-ray images	24 patients in 64 treatments	Intrafraction	2.6 ± 1.3	2.3 ± 1.0	2.8 ± 1.1
Gutfeld (26)	SBRT spinal involvement	CBCT	14 patients	Interfraction	0.38 ± 1.21	−0.51 ± 2.0	1.12 ± 1.82
As above				Maximum interfraction values	−4.29	−6.64	5.76
Ito (12)	Gastrointestinal stromal tumor	Ultrasound	1 patient	Rotation during respiration; maximum rotation >30°, axis not mentioned			
Noel (10)	Prostate	Electromagnetic tracking	1 patient over 40 fractions (80 min)	Intrafraction; maximum 27°	8 ± 7	1 ± 2	2 ± 1
Li (15)	Prostate	Electromagnetic tracking	319 randomly selected fraction from 29 patients	Intrafraction	1.5 ± 5.2	0.4 ± 1.7	0.8 ± 1.6
De Boer (27)	Prostate	Electronic portal image (EPI) with 4 platinum markers	15 patients on average 17 fractions/patient	Interfraction	3.1 ± 4.9	0.8 ± 1.0	0.0 ± 1.5
Aubry (28)	Prostate	EPI	7 patients, 348 fractions	Interfraction	6.1 ± 5.6	2.8 ± 2.4	2.0 ± 2.2
As above			7 patients, 44 fractions	Intrafraction	1.8 ± 1.0°	1.1 ± 0.8	0.6 ± 0.3
Burch (29)	Prostate	Electromagnetic tracking	11 patients	Intrafraction, up to 10° rotation correlated to translation, rotation axis not mentioned			
Dehnad (30)	Prostate	CT and EPI	10 patients	Systematic interfraction	0.5 ± 4.7	−0.5 ± 2.0	−1.0 ± 2.7
As above				Random interfraction	0.5 ± 3.6	−0.5 ± 1.7	−1.0 ± 1.9
Van de Heide (31)	Prostate	EPI	234 patients	Systematic interfraction	−0.2 ± 6.8	0.04 ± 2.8	−0.3 ± 2.8
As above				Random interfraction	−0.2 ± 3.1	0.04 ± 2	−0.3 ± 1.7
Balter (32)	Prostate	Film	10 patients	Interfraction	0.7 ± 3.2	0.2 ± 0.7	
Beck (33)	Prostate	EPI	10 patients	Interfraction maximum values	17.7	20.9	5.6
Stroom (34)	Prostate	CT	15 patients	Interfraction prone and supine (averaged)	4.6 ± 3.4	1.3 ± 1.5	1.0 ± 0.9
Steenbakkers (35)	Prostate	MRI	10 volunteers, 5 MRI scans in four different positions	Interfraction, cause with/without knee support. CC/AP rotation insignificant.	5.6	–	–
Hoogeman (16)	Prostate	CT	19 patients with 8–13 repeat CT scan	Interfraction	5.1 ± 3.6	2.2 ± 2.0	1.3 ± 1.6

Abbreviations: AP = anteroposterior; CC = craniocaudal; CT = computed tomography; EPI = electronic portal image; LR = left-right; MRI = magnetic resonance imaging.
Values are averages unless otherwise specified in comments.

Table 2. Summary of geometric accuracy for fixed rotated target measurements

Target rotation angle (°)	Beam aperture rotation (°)	Beam-target rotational alignment difference (°)
5.6	5.1	−0.5
10.1	10.2	0.0
15.6	15.0	−0.6
20.5	20.1	−0.3
25.1	25.2	0.1
30.6	30.2	−0.4
40.7	39.9	−0.8
44.8	45.3	0.5
50.1	50.3	0.1
55.7	55.1	−0.6
Combined		−0.3 ± 0.6 (1 SD)

Table 3. Summary of geometric accuracy for actively rotating target experiments

Summary	Target rotation from 0° to 60°			Target rotation from 60° to 0°		
	Exp 1	Exp 2	Exp 3	Exp 1	Exp 2	Exp 3
Average beam-target rotational difference (°)	1.2	1.7	0.6	−0.4	−1.7	0.2
SD (°)	0.6	0.8	0.5	0.6	0.6	0.6
Combined over 3 experiments (°)	1.2 ± 0.8			−0.6 ± 1.0		
Combined over 6 experiments (°)	0.3 ± 1.3					

Table 4. Summary of treatment delivery efficiency with different target rotation angles

Treatment efficiency	15° rotation	30° rotation	45° rotation	60° rotation	Active rotation
Conformal beam	100%	100%	100%	90.4%	85.7%
Intensity-modulated radiotherapy beam 1	90.0%	80.5%	76.7%	65.7%	81.2%
Intensity-modulated radiotherapy beam 2	98.0%	93.5%	88.9%	81.6%	87.7%

The delivery efficiency is defined as the percentage of the time to deliver the reference beam divided by the time taken to deliver the beam accounting for rotation.

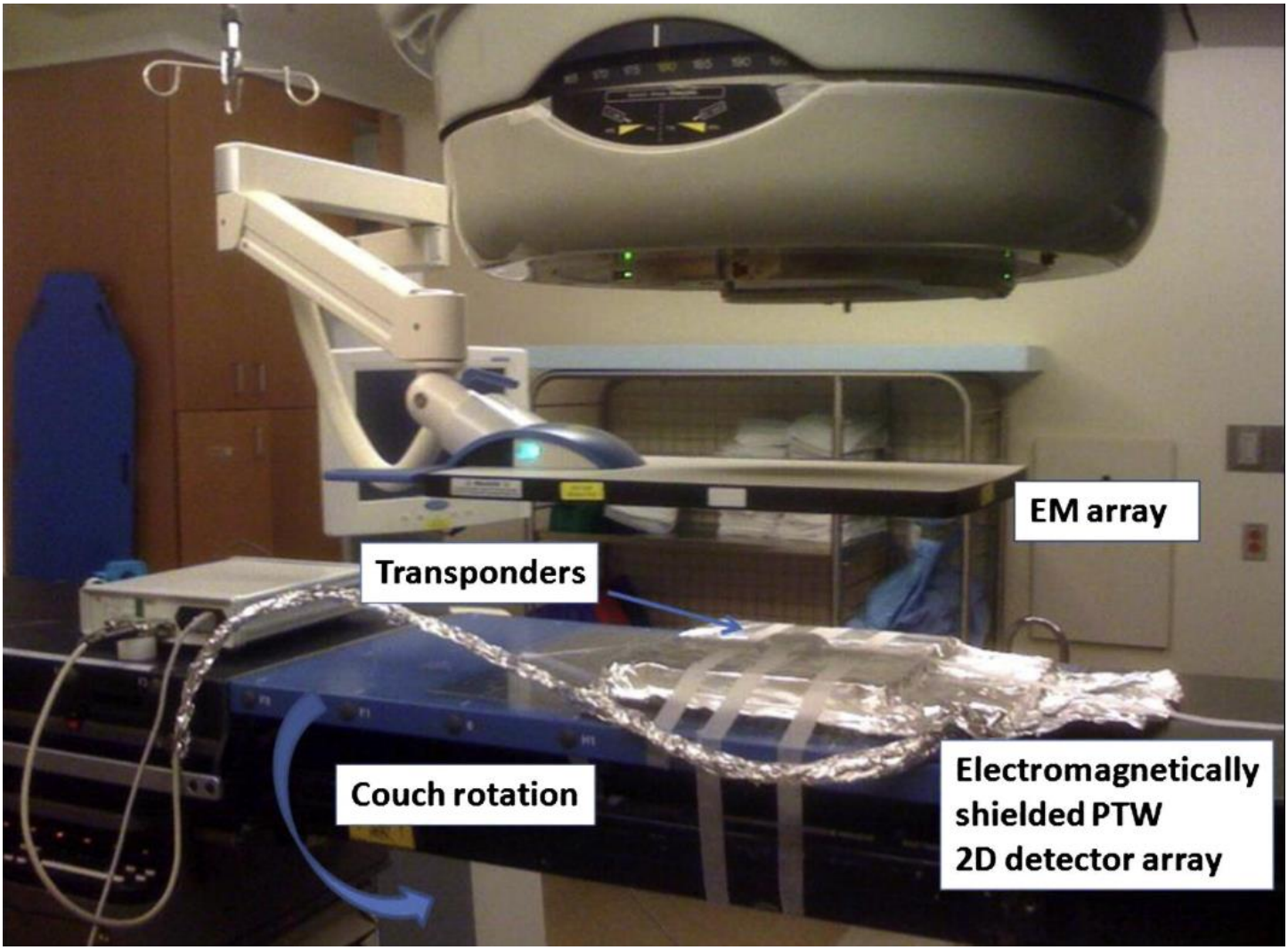

Fig. 1. Experimental setup: the target rotation was performed by rotating the couch with electromagnetic transponders and an electromagnetically shielded PTW two-dimensional ion chamber array. The beam rotation was controlled by a real-time dynamic multileaf collimator tracking system taking the transponder rotation measurements as input.

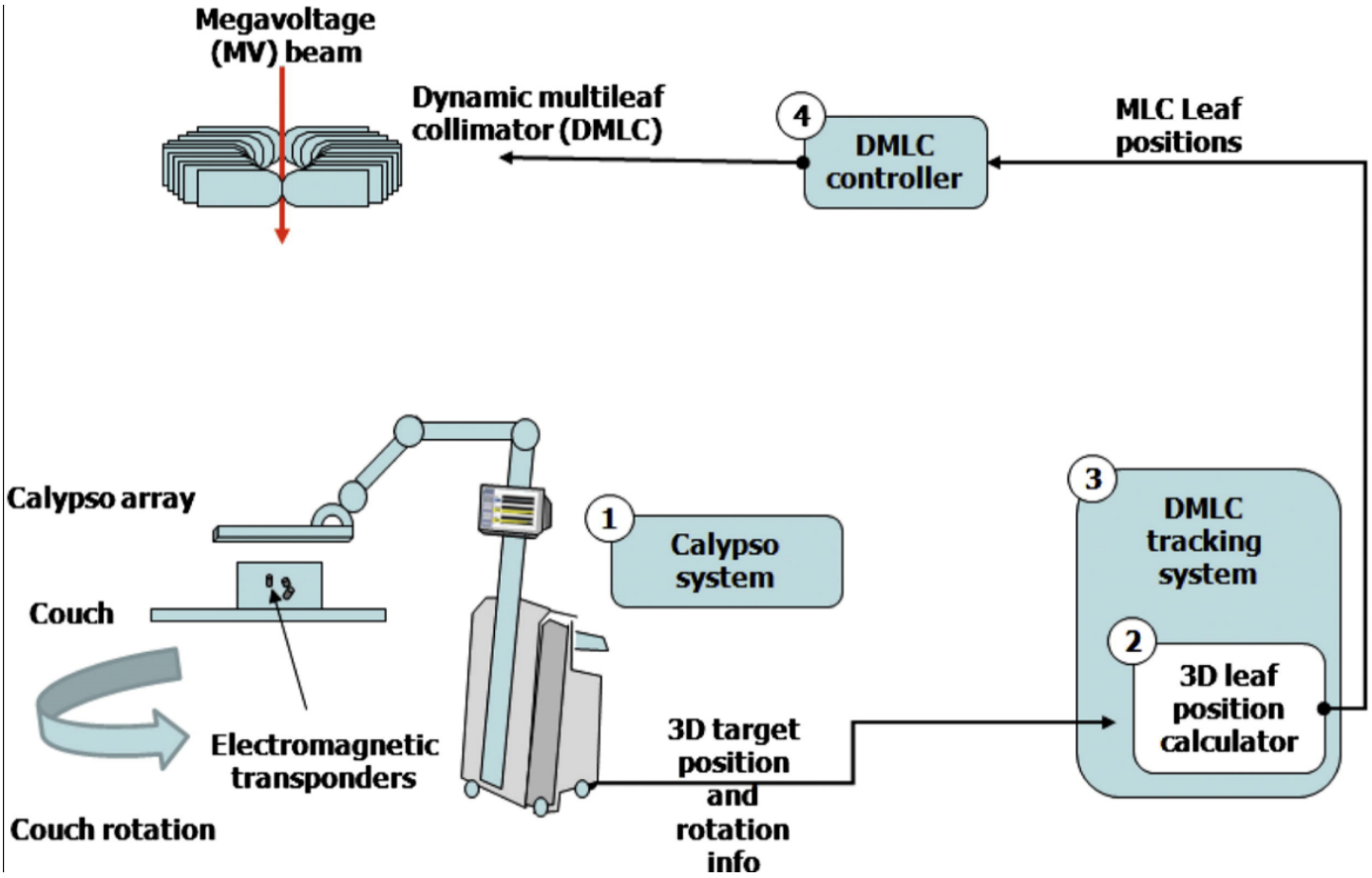

Fig. 2. Flowchart of electromagnetically guided real-time dynamic multileaf collimator rotation tracking.

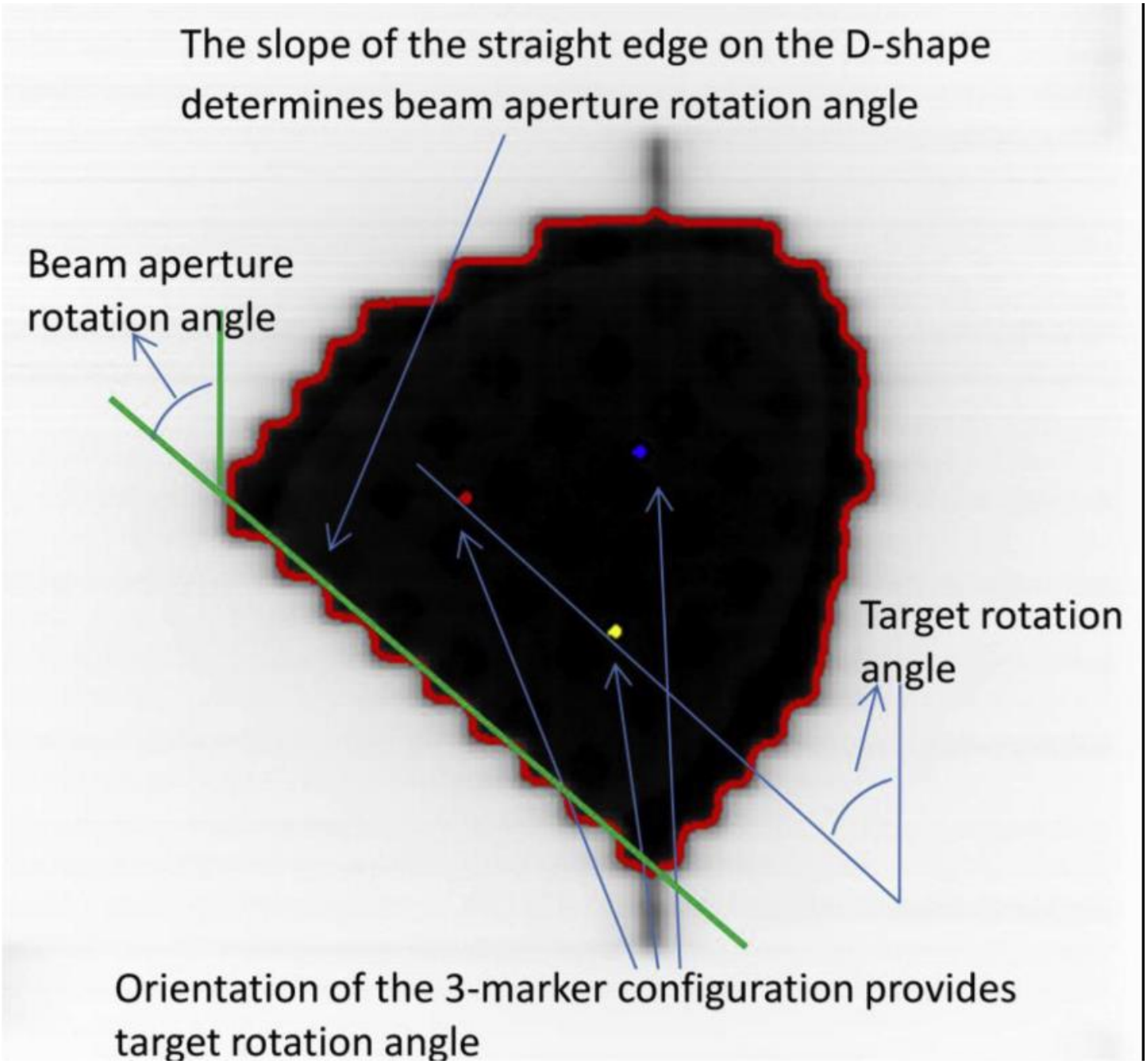

Fig. 3. The geometric accuracy was measured using the electronic portal imaging device. The target rotation angle was determined by the orientation of the embedded markers. The beam aperture rotation angle was estimated from the slope of the straight edge on the D-shape. The beam-target rotational alignment difference is the difference between the beam aperture rotation angle and the target rotation angle.

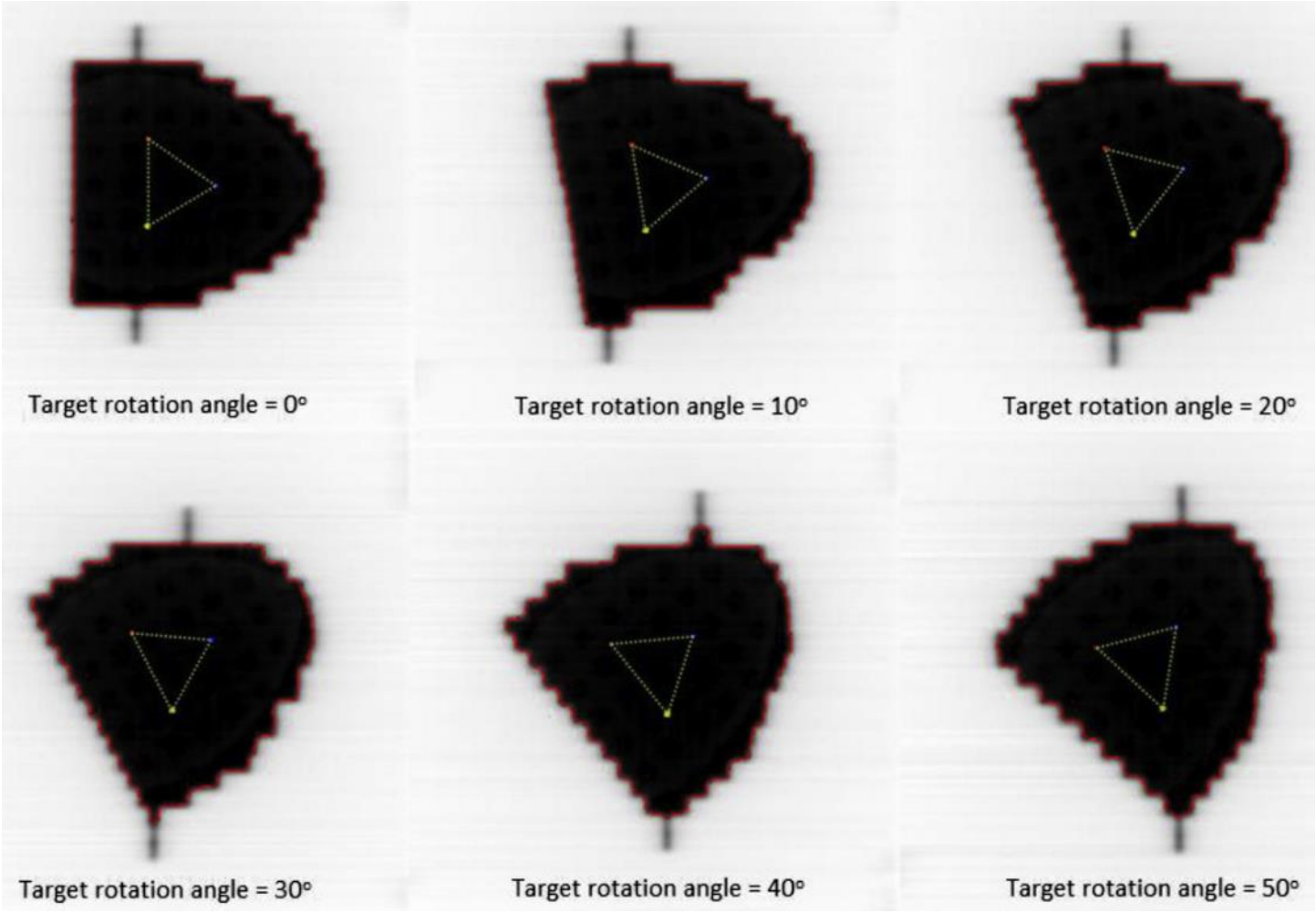

Fig. 4. Example electronic portal imaging device images, showing the radiopaque markers representing the target rotation and the beam rotation shown with the multileaf collimator aperture (red outlines). Target rotation can be clearly observed through the green triangle rotation, which is formed by three markers (red, blue, and yellow).

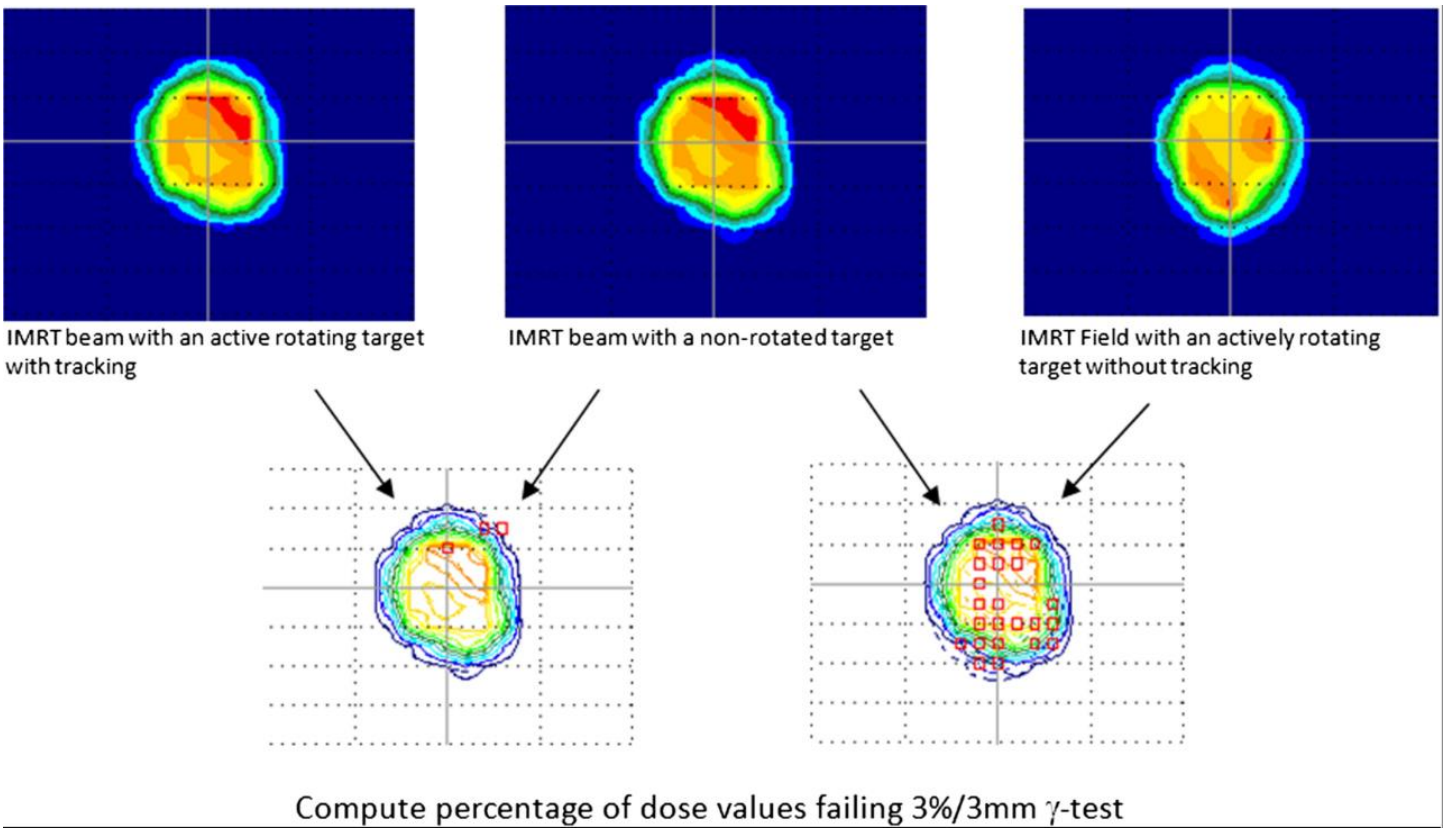

Fig. 5. Example of dosimetric comparison: dosimetric measurement of an intensity-modulated radiotherapy (IMRT) beam with an actively rotating target with tracking (upper left) and rotating target without tracking (upper right) were compared with the reference dosimetric measurement of the same IMRT beam with a nonrotated target (upper middle) using a the 3%/3 mm γ-test. The isodose comparison results are shown in the bottom row.

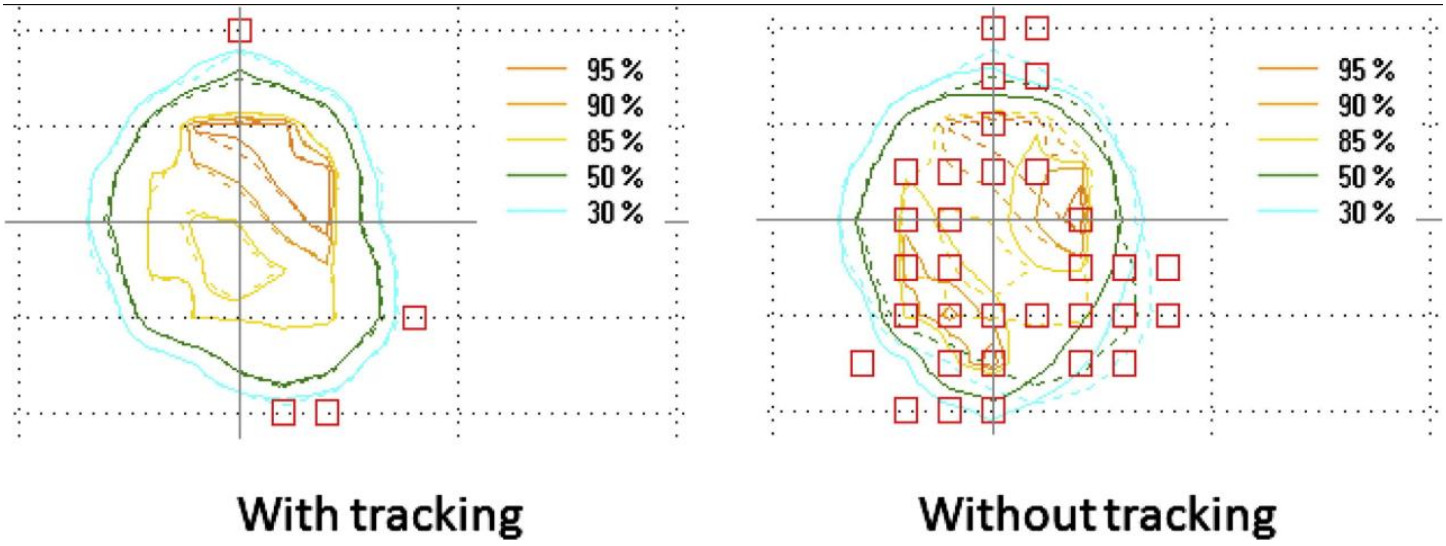

Fig. 6. Example of high-dose region isodose curves for an intensity-modulated radiotherapy field. The red squares indicate points failing the 3%/3 mm γ-test. Left: actively rotating target with tracking (solid lines); nonrotated target (dashed lines). Right: actively rotating target without tracking (solid lines); nonrotated target (dashed lines).

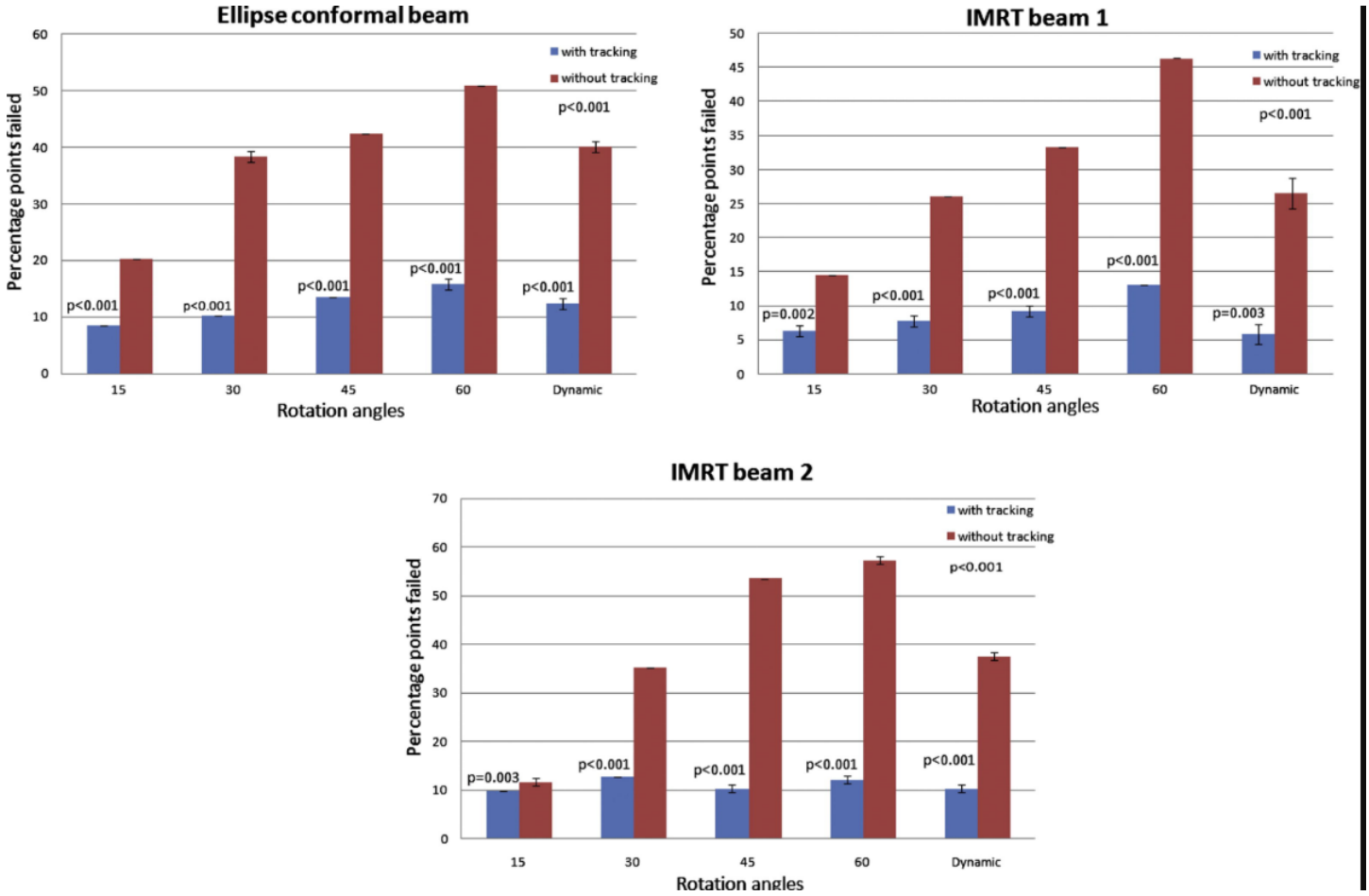

Fig. 7. Dosimetric result summary: the percentage of dose values that failed the 3%/3 mm γ-test with and without tracking for conformal and intensity-modulated radiotherapy beams.